Journal of Molecular Liquids 368 (2022) 120745

Contents lists available at ScienceDirect

Journal of Molecular Liquids

journal homepage: www.elsevier.com/locate/molliq

A biophysical study of DNA condensation mediated by histones and protamines

Bruna B.S. Souza [a,1], Thiago C. Lourenço [a,1], Barbara B. Gerbelli [b], Pedro L. Oseliero Filho [c], Cristiano L.P. Oliveira [c], Antonio Miranda [a], Emerson R. da Silva [a,*]

[a] Departamento de Biofísica, Universidade Federal de São Paulo, São Paulo 04023-062, Brazil
[b] Centro de Ciência Naturais e Humanas, Universidade Federal do ABC, Santo André 09210-580, Brazil
[c] Instituto de Física, Universidade de São Paulo, São Paulo 05508-090, Brazil

ARTICLE INFO

Article history:
Received 6 June 2022
Revised 17 October 2022
Accepted 1 November 2022
Available online 7 November 2022

Keywords:
DNA condensation
Nucleoprotein
Self-assembly
Small-angle scattering
Atomic force microscopy
Nanospectroscopy

ABSTRACT

The compaction of long DNA strands into confined spaces such as the nuclei of eukaryotic cells is an essential phenomenon towards the emergence of elaborated forms of life. Histones and protamines are the major nucleoproteins involved in this task participating in the formation of chromatin in somatic and germinative cells, respectively. In addition to a fundamental understanding of critical biological processes, DNA condensation also holds strong potential in biotechnology. Herein, we investigate the mesoscale structure of complexes formed between DNA and histones or protamines. A sophisticated set of biophysical methods encompassing steady-state fluorimetry, small-angle X-ray scattering and infrared nano spectroscopy was used to unveil both the self-assembly and molecular interactions of these complexes. We explored the fluorescence of a molecular rotor, thioflavin T, to investigate the accessibility of ligands in the inter-base environment of DNA strands. AFM-based infrared spectroscopy was used for the first time to probe the vibrational signature of individual DNA/nucleoprotein nano assemblies and disclose secondary-structure features. Our results show that protamines form highly compact structures in which DNA folding hinders access to the inter-base spacing. These assemblies exhibit diversified secondary-structure conformations, with the presence of β-sheets stabilizing the packing. In contrast, histone-based complexes are characterized by fibrillar nano assemblies exhibiting larger inter strands separations and access to guest molecules that intercalate between bases. The findings presented here may help the understanding of DNA condensation mediated by these two major nucleoproteins and may assist the optimization of gene vehicles based on these promising nano assemblies.

1. Introduction

The compaction of long DNA strands into confined spaces is a ubiquitous phenomenon in biology and a crucial step towards the emergence of elaborated forms of life. This intricate framework involves multiple physicochemical steps that depend on the association of DNA with various biological ligands, such as small ions, natural polyamines, lipids, and nucleoproteins.[1–5] Striking examples of extreme condensation are observed in the self-assembly of chromatin in eukaryotic cells and the packing of viral genomes within lipoprotein capsids.[6,7] This challenging process leads to functional assemblies that fit within tiny compartments and maintain the storage, regulation and transcriptional capabilities of genes. Nucleoproteins are highly specialized structures for this task, with histones and protamines being described as the major players in DNA condensation.[2,8,9] Histones are the main ones responsible for DNA condensation in somatic cells leading to the formation of nucleosomes and organization of chromatin,[10–12] whereas, in germinative cells, they are replaced by protamines.[13,14] These nucleoproteins are highly cationic polyelectrolytes, and their interaction with DNA occurs mainly through electrostatic attraction between basic residues at protein strands and phosphate groups at the nucleotide backbone.[13] Protamines are arginine-enriched proteins, whereas histones comprise lysine amino acids.[15] In addition to fundamental studies on chromatin structure and gene regulation, DNA condensation mediated by histones and protamines attracts interest due to their potential in biotechnology.[11] The development of non-viral vectors for gene therapy and designing DNA-based self-assemblies are topic

* Corresponding author.
E-mail address: er.silva@unifesp.br (E.R. da Silva).
[1] These authors contributed equally to this work.

https://doi.org/10.1016/j.molliq.2022.120745
0167-7322/

subjects whose development strongly depends on a deep understanding of DNA compaction.[3,16–19].

From understanding fundamental biological phenomena to the development of biomedical applications, DNA condensation has attracted great interest in the research community, leading to many studies addressing the topic. However, such works rarely explore the self-organization process on a hierarchical scale, approaching the physicochemical aspects of the DNA/nucleoprotein interaction across scales covering from the molecular level to the micrometric range. In this work, we investigated in detail the mesoscopic structure of model systems formulated through the complexation of DNA with histones and protamines to provide comparative analyses between self-assemblies formed by these two major nucleoproteins. A sophisticated set of experimental techniques gathering steady-state fluorimetry, small-angle X-ray scattering and infrared nano spectroscopy was used to unveil both the self-assembly and molecular interactions of these complexes with particular attention to the supramolecular arrangements resulting from complexation. We explore the fluorescence of a molecular rotor, thioflavin T, to investigate the interaction between DNA and nucleoproteins to extract valuable information on the accessibility of ligands to the inter base environment of DNA strands. For the first time, AFM-based infrared spectroscopy was used to study the vibrational signature of individual DNA/nucleoprotein nano assemblies. Our results show that protamines form highly compact structures, wherein DNA folding hinders access to the inter-base spacing. These assemblies exhibit diversified secondary-structure features, with β-sheets stabilizing the package. In contrast, histone-based complexes are characterized by fibrillar nano assemblies exhibiting larger inter strands separations and access for guest molecules intercalating between bases.

2. Materials and methods

2.1. Reagents and sample preparation

All reagents were purchased from Sigma-Aldrich and used as received. The nucleic acids fraction was composed of double-stranded calf-thymus DNA containing linear nucleotide chains (product code D1501), with an average molecular weight <Mw> = 660 Da per base pair. Gel electrophoresis revealed the presence of polydisperse chains with sizes between ~3 kbp and 20 kbp, with most strands remaining around 15 kpb. The histones also originated from calf-thymus, and they corresponded to whole unfractionated histones (product code H9250) containing a mix of four fractions associated with core histones H2a, H2b, and H4, with <Mw> = 15 kDa. Protamines were originated from salmon sperm and purchased in the form of sulfate salt (product cod. P4020). They are composed of P1 and P2 type protamines, with <Mw> = 4.5 kDa. DNA and nucleoproteins were received as a lyophilized powder, and stock solutions were prepared by weighing the appropriate amounts of biomolecules and dissolving them with ultrapure water. To avoid degradation, the solutions were prepared using nuclease-free tubes and pipettes, and only fresh stocks (i.e., <24 h from solubilization) were used in sample preparation. UV–Vis measurements revealed $A_{260}/A2_{80}$ ratios between 1.8 and 1.85 for all batches used throughout the work, confirming the purity of DNA in the samples.[20] The concentration of DNA stocks was ascertained by determining the absorbance at 260 nm (A_{260}) and considering an average extinction coefficient of 13200 M^{-1}. cm^{-1}. [21] The final concentrations were obtained from the corresponding dilutions used for preparing DNA/nucleoprotein mixtures. A series of samples in our study has been prepared using ultrapure water as a solvent, with DNA-nucleoprotein solutions at native pH. This approach has been followed in previous works dealing with nucleic acid-nucleoprotein interactions[4,16], and the choice aims to avoid specific and non-specific interactions between the macromolecular species and buffer compounds. The native pH of the stock solutions was found to be 5.8 for DNA, 4.8 for histones, and 4.7 for protamines. Another series of samples have been investigated using HEPES (10 mM, pH = 7.2) or TE buffer (10 mM Tris, 1 mM, pH = 7.2) to mimic the pH conditions found in cell nuclei.[22] Complexes were then prepared by mixing the corresponding amounts from fresh stocks to obtain the desired DNA/protein ratios and concentrations.

2.2. EtBr displacement assays

Ethidium bromide (EtBr) displacement assays were performed to analyze the interaction between DNA and ligands (protamines and histones). Aqueous solutions were prepared with 15 μM DNA and 2.5 μM EtBr, then mixed in test tubes with nucleoproteins covering concentrations in the interval 0–3.5 μM. The native pH of DNA-histone solutions was 5.1 ± 0.2, and the native pH of DNA-protamine samples was 4.8 ± 0.2. The mixtures were submitted to vigorous vortexing and left at rest for two hours prior to measurements. The excitation wavelength was set at λ_{exc} = 520 nm, and emission spectra were recorded in the interval 550 < λ_{em} < 700-nm. Intensity values at 590 nm were plotted as a function of ligand concentration, revealing sigmoidal profiles that were successfully described by the Boltzmann's equation:[23,24].

$$I_{590} = I_{sat} + \frac{I_0 - I_{sat}}{1 + e^{\frac{(C - C_0)}{dC}}} \quad (1)$$

where I_0 and I_{sat} correspond, respectively, to the initial intensity (solution without ligand) and to the intensity reached when ligand/DNA association saturates, C is the concentration of ligand, C_0 is the midpoint concentration of the sigmoid, and dC is the transition width between the asymptotic regimes.

2.3. ThT fluorescence

The fluorescence behavior of thioflavin T (ThT) in the presence of ligand/DNA complexes was monitored to probe the interaction between proteins and DNA. All samples were prepared in solutions containing 30 μM ThT.[25] Two series of titration experiments were performed: In the first one, the concentration of DNA base pairs was kept at 15 μM and nucleoproteins were titrated in intervals of 0–3 μM (for protamines) or 0–1 μM (for histones). pH measurements of these titration series in ultrapure water indicated values at 5.3 ± 0.3. In the second assay, nucleoprotein solutions at 1.3 μM were co-solubilized with ThT, and DNA was titrated in the interval 0–20 μM. Fluorescence spectra were recorded on a Shimadzu F-2500 fluorimeter exciting the samples at λ_{exc} = 440 nm, and emission data were registered in the range 450 nm < λ_{em} < 600 nm. All experiments were performed at room temperature, and a magnetic stirrer bar was activated during data collection to homogenize the mixtures.

2.4. AFM-based infrared spectroscopy (AFM-IR)

Nano spectroscopy measurements were performed using an Anasys NanoIR2-s apparatus as described elsewhere.[25–27] DNA/nucleoprotein complexes were prepared by mixing DNA and nucleoproteins from stock solutions at the same concentrations used in fluorescence assays. The final DNA concentration in the mixtures was 15 μM, whereas nucleoprotein concentration was kept at 4 μM. At these concentrations, no precipitation was observed, and solutions appeared transparent to the eye. Droplets from these mixtures were deposited on Au-coated silica substrates

and left at rest for about 5 min before removing the excess solution with a paper filter. The substrates were incubated overnight in evacuated desiccators prior to further analysis to ensure complete drying of the samples. The microscope was operated in contact mode, and the first step was to collect topography images covering $3 \times 3\ \mu m^2$ or $5 \times 5\ \mu m^2$ areas (512×512 pixels). This step served to reveal the morphology of complexes on the substrates and to identify regions of interest (ROIs). In the second step, the AFM tip (~30 nm radius) was positioned on top of ROIs and spectra were collected in the interval between 1500 cm^{-1} and 1800 cm^{-1}. This procedure allowed us to investigate the spectral signature of different nanoparticles and to discriminate the infrared behavior of different regions within a single nanoparticle. All data were baseline subtracted and smoothed using an FFT filter (5 points of window). Data analysis was performed using the AnalysisStudio software and further visualization enhancement was carried out with the Gwyddion.[28].

2.5. Polarized Light Microscopy (PLM)

Polarized light microscopy was used to probe the liquid crystalline features and amyloidogenic characteristics of the samples. Mixtures containing DNA and proteins at concentrations of 3 mg/ml were sandwiched between glass slides and cover slips. The samples were observed on a Nikon E200 Eclipse microscope endowed with a crossed polarizers setup. Specimens have been examined using 20 X objectives, and the instrument was coupled to a CCD device to register images.

2.6. Small-angle X-ray Scattering (SAXS)

Small-angle X-ray scattering assays were carried out on the SAXS-1 beamline at the Brazilian Synchrotron Light Laboratory (LNLS, Campinas). Nucleoprotein/DNA mixtures were prepared in water at final concentrations of 1 mg/ml. Under these conditions, the formation of white pellets was observed, which were sandwiched between Kapton foils inside a 1 mm pathlength cell holder. To analyze uncomplexed controls containing only DNA or nucleoprotein, 300 μL from the solutions were injected between mica windows and examined in the same manner as performed for the pellets. X-ray energy was kept at 8 keV (λ = 1.54 Å), and a Dectris 300 K Pilatus detector was positioned at 100 cm from the sample holder. The setup was fully calibrated by using scattering profiles from silver behenate standards. This configuration enabled access to scattering vectors in the interval $0.13\ nm^{-1} < q < 4\ nm^{-1}$ (where $q = 4\pi/\lambda\ \sin\theta$). Ten frames of 30 s each were collected and compared to each other to check for radiation damage. The frames were then averaged and a scattering profile from the cell containing only water was used for background subtraction. The resulting datasets were characterized by Porod-like decaying at the low-q region, featuring sharp interfaces between particles and the surrounding solvent,[29] and by interference peaks at the intermediate-to-high q-values, indicating the presence of correlation domains in the inner structure of aggregates. Full-range data fitting was carried out using the SASFit program[30] with the following functional form:

$$I(q) = A \cdot q^{-\alpha} + B \cdot q^{-\beta} + \frac{C}{1 + (|q - q_0|\xi_0)^2} + \frac{D}{1 + (|q - q_1|\xi_1)^2} + Bkg \quad (2)$$

In Eq. (2), the first and second terms are power laws accounting for features observed at the low and intermediate q-regions, whereas the third and fourth terms are broad peak functions.[31] Bkg is an additive constant to describe a flat background related to electronic noise and incoherent scattering. Parameters A, B, C and D are scaling constants to adjust the weight of each component in the model. The exponents α and β carry information on the global form of the particles. Values closer to 0 are usually associated with globular shapes, and values near to 1 indicate elongated structures (e.g., rod-like shapes).[31,32] These exponents can also be associated with the fractal dimension of the scatters, and thus, the information on the nature of fractal aggregates could be devised.[33] The fractal dimension is determined as follows:

$$\alpha = D_m, \quad for \quad 1 < \alpha < 3 \quad (3)$$

$$\alpha = 6 - D_s, \quad for \quad 3 < \alpha < 4 \quad (4)$$

where D_m corresponds to the dimension of mass fractals and D_s to the dimension of surface fractals. In our study of highly concentrated condensates, we have observed only the formation of surface fractals. In the broad peak terms, q_0 and q_1 correspond to peak positions associated with the average distance d between scattering inhomogeneities through Bragg's law, $d = 2\pi/q$. The parameter ξ is a correlation length associated with the broadness of the peak and brings information on the ordering of the structure: the broader the peak the smaller the correlation length, and the lower the degree of order in the assemblies. Data analysis was carried out with the SASFit using Eq. (2) to fit the data.

3. Results and discussions

3.1. EtBr displacement assays

Ethidium bromide (EtBr) displacement assays were performed to investigate the interaction between DNA and the nucleoproteins. It is widely known that EtBr binds to nucleic acids with high affinity, enhancing in this way its own fluorescence.[34] Herein, the fluorescence yield can be used to probe the competition between nucleoproteins and the dye for binding sites at DNA duplexes. In Fig. 1A, fluorescence profiles from complexes prepared with protamines are characterized by a maximum at ~590 nm which is found to decay to about 20% of the initial fluorescence upon the addition of nucleoprotein to the mixture, indicating that EtBr molecules are released from the DNA strands into the bulk solution. In 1B, the EtBr fluorescence is shown for complexes formed between DNA and histones. Again, one observes fluorescence decay upon the increase of nucleoprotein concentration; however, although the fluorescence yield is found to decrease upon the addition of histones, we now observe that the decay is much smoother than in protamine solutions, and intensities reach a plateau at ~40% of the initial emission. To quantitatively describe this behavior, the relative intensity at 590 nm was plotted as a function of the nucleoprotein concentrations (Fig. 1C), and the resulting curves have a "Z" shape which was properly fitted to the sigmoid function described in Eq. (1). The midpoint of the curve for protamine complexes was found at C_{0_Prot} = (1.31 ± 0.13) μM whereas for histone complexes it was at C_{0_Hist} = (0.71 ± 0.27) μM.

C_0 can be used as an estimate for the apparent dissociation constant, K_D, being therefore proportional to it. The smaller the K_D value (and thus C_0) the higher the binding affinity. In addition, by assuming that the dissociation of EtBr occurs due to the occupation of binding sites by the ligand, C_0 also provides an estimate of the association between the nucleoproteins and DNA. Putting the findings together, we may conclude that histones are less efficient at folding nucleotide chains. In fact, EtBr fluorescence in the presence of protamines remarkably drops to ~20% of its initial level, thus suggesting that a lower number of interaction sites remain available on DNA strands and indicating more compact assemblies in comparison with DNA/histones complexes. EtBr displacement assays performed in ultrapure water at 37 °C revealed fluorescence

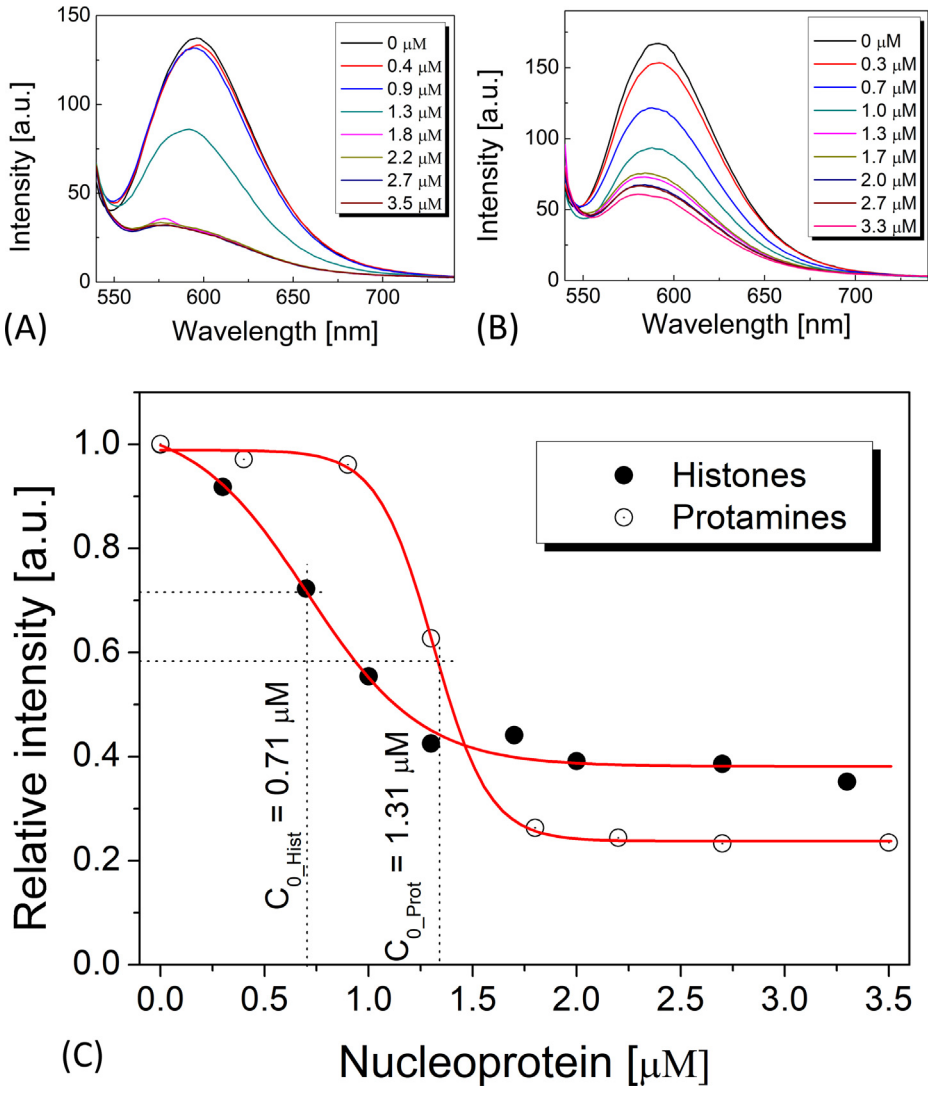

Fig. 1. EtBr displacement assays in DNA/nucleoprotein solutions (native pH, room temperature). Fluorescence spectra from samples containing (A) protamines or (B) histones. (C) Fluorescence intensities (relative to nucleoprotein-free controls) as a function of nucleoproteins concentration. Red lines are sigmoidal fits according to Eq. (1).

profiles very similar to those observed at room temperature (see SI File, Fig. S1), suggesting that temperature variation within the physiological range has minor effects on the interplay between DNA and nucleoproteins. When the analyzes are performed in buffered solutions at pH = 7.2 (Figs. S3 and S5), the capacity of protamines to displace EtBr from DNA strands is found to be even stronger than in ultrapure water, as indicated by the level of fluorescence at the saturation plateau (~20% of the initial value in ultrapure water, and less than 10% at pH = 7.2). In the case of histones, the displacement level remains essentially the same (~40 % of the starting value), suggesting that interactions between DNA and histones are barely affected by pH. Indeed, the apparent dissociation constants (parameter C_0 in Eq. (1)) of protamines decreases from C_{0_Prot} = (1.31 ± 0.13) μM in water to C_{0_Prot} = (0.91 ± 0.17) μM in TE, whereas for histones this parameter slightly increases within uncertainties from C_{0_Hist} = (0.71 ± 0.27) μM in water to C_{0_Hist} = (0.86 ± 0.24) μM in buffer.

3.2. ThT fluorescence in the context of DNA-nucleoproteins binding:

The DNA/nucleoprotein interaction was also investigated using thioflavin T (ThT) fluorescence assays. Recently, the applications of ThT as a fluorescence probe have expanded far beyond the study of amyloids and have also gained importance in conformational analyses of nucleic acid assemblies.[35] Upon intercalation between DNA bases, the molecular rotor formed by ThT benzothiazol and dimethylaminobenzyl rings undergoes steric hindrance, decreasing non-radiative dissipation during de-excitation steps and increasing the fluorescence quantum yield.[36,37] This feature makes ThT very sensitive to microviscosity in the vicinities of DNA duplexes, making it an excellent reporter for local conformational changes in the DNA chain.[38] In Fig. 2A, one observes that ThT fluorescence increases about one order of magnitude in the presence of DNA (compare bold curves in 2A). Peaks characterize the data at 485 nm, and spectra from DNA/protamine solutions containing ThT indicate that fluorescence intensities decrease dramatically as the fraction of protamine increases in the mixture. This behavior is similar to that observed in the EtBr assays above, thus suggesting that protamine also promotes the displacement of ThT. Moreover, the plot of fluorescence intensity as a function of protamine concentration (Fig. 2B) also has a sigmoidal shape with an inflection point at C_0 = 1.08 ± 0.01 μM, very close to the value obtained in EtBr assays. Control experiments evaluating the ThT fluorescence in the presence of nucleoproteins do not indicate fluorescence

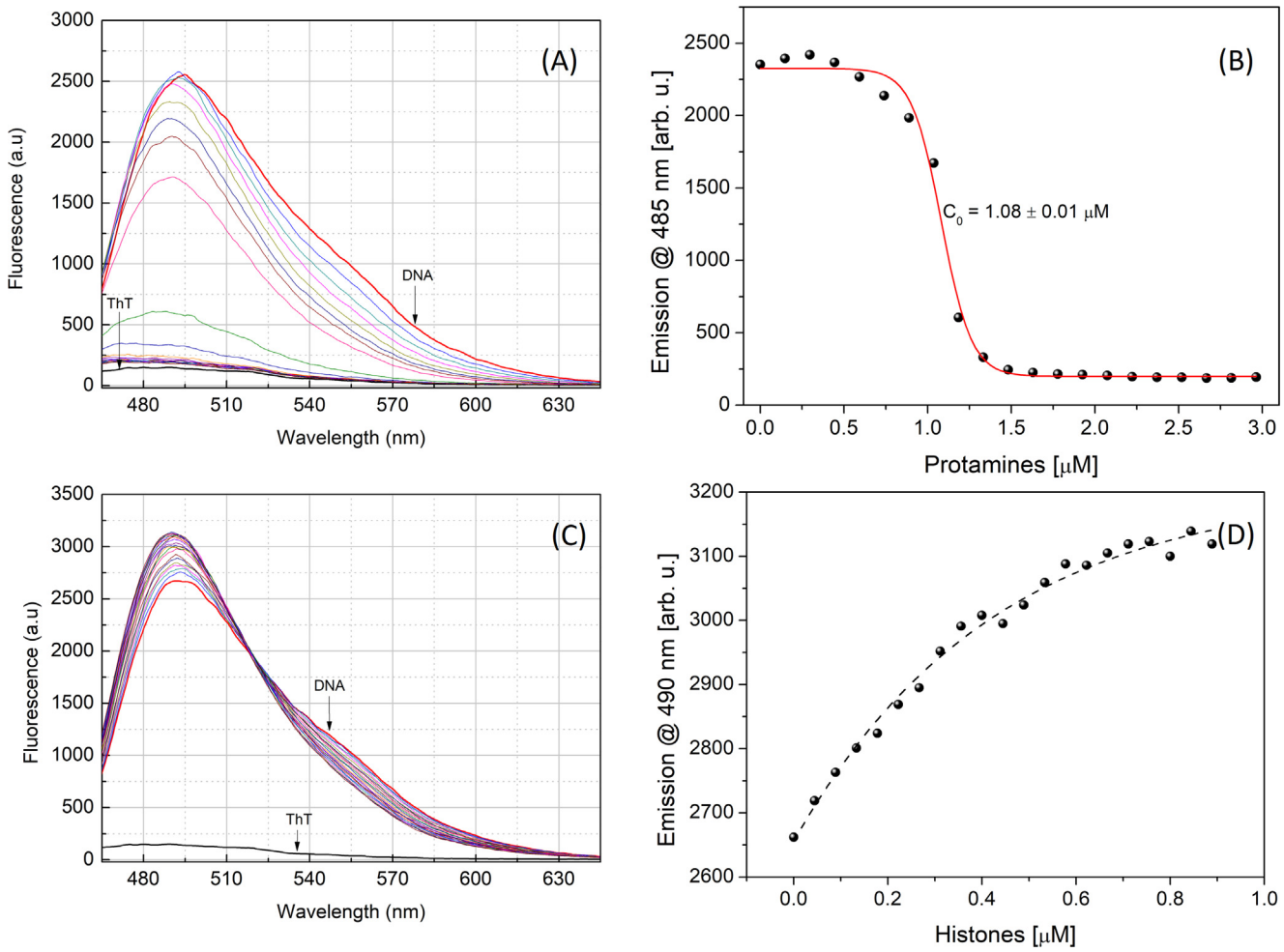

Fig. 2. (A) Emission spectra of ThT and (B) intensity vs. nucleoprotein concentration from DNA/protamine samples. The sigmoidal fitting has been performed using Eq. (1). (C) ThT fluorescence spectra and (D) intensity vs. histone concentration from DNA/histone solutions. The dashed line is a guide to the eye showing the exponential behavior of ThT emission.

growth within the concentration regime used in the study; thus, changes in the quantum yield of the dye are related to modifications in the interaction between ThT and DNA, likely due to conformational changes induced by the ligands.

In contrast to DNA/protamine complexes, in DNA/histone samples ThT fluorescence is found to grow upon the addition of histone to DNA solutions (Fig. 2C). In addition, a hypsochromic effect is observed, and the emission peak is found to blue shift to 490 nm. The plot of maximum intensities as a function of histone concentration, Fig. 2D, exhibits a monotonic increase with an exponential shape. Therefore, we may conclude that the binding of histone to DNA chains is insufficient to promote displacement of ThT, and the conformational arrangements of the strands are different from those observed in protamine complexes. Instead, histones likely contribute to stabilizing ThT molecules intercalated in the DNA structure by inducing conformations that favor the accessibility of the dye to the inter-base environment. As seen below, the nanoscale morphology of condensed complexes is quite different depending on the nucleoprotein used in the condensation.

Distinct effects of protamines and histones on ThT fluorescence upon binding to DNA were further evidenced in assays in which the concentration of nucleoproteins was fixed, and the DNA was titrated into solution. In Fig. 3A, DNA titration into the solution containing only ThT shows a significant increase in fluorescence upon the addition of DNA. Across the concentration range studied (i.e., 0–20 μM DNA), the yield linearly increased and reached values about 12 times higher than the emission from the solution containing only ThT. When ThT appears co-solubilized with protamines (Fig. 3B), the behavior is quite different and the fluorescence yield remains nearly constant upon DNA titration, evidencing that protamines hinder the association between the dye and DNA strands. For solutions where histones are co-solubilized with ThT, Fig. 3C, fluorescence spectra are found to blue shift, and emission intensities grow by a factor of about 20×. The different behaviors are evidenced in Fig. 3D, where the maximum intensities are plotted as a function of DNA concentration in the mixtures. We observe that intercalation of ThT in DNA strands enhances the fluorescence of the dye and that protamines and histones affect the binding in very distinct manners. Whereas protamines drop fluorescence growth likely due to competition with ThT binding sites, histones reinforce the emission of the dye, probably due to stabilization of the ThT rotor upon intercalation in ordered assemblies.[35] It should be noted that at low DNA concentrations, fluorescence yield in DNA/histone solutions also exhibits a near-constant feature. We ascribe this behavior to the initial binding of histones to DNA, which first promotes the occupation of ThT sites; however, as the fraction of DNA in the solution increases, ordered clusters appear in the complexes, and ThT molecules can

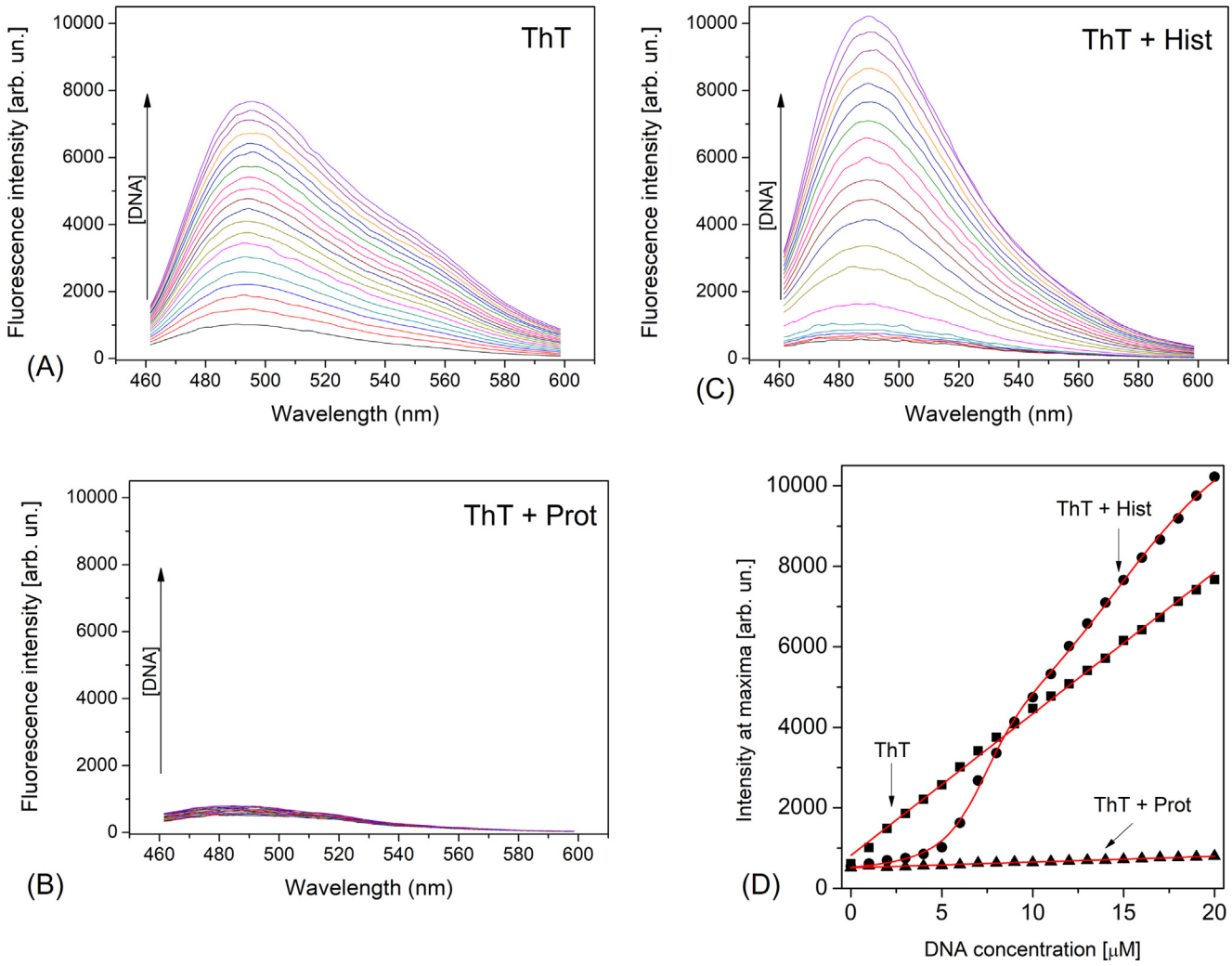

Fig. 3. DNA titration assays in solutions containing ThT and nucleoproteins. DNA titration in a ThT solution (A), ThT + protamines mixture and (C) ThT + histones solution. All plots are present at the same scale for comparison. (D) Maximum intensities as a function of DNA concentration. The red lines are a guide to the eye.

intercalate. As such, the molecular rotor in the ThT chromophore is rotor stabilized, and the fluorescence yield is enhanced. Similar to EtBr assays, data obtained at 37 °C exhibit the same profiles found at room temperature (Fig. S2), confirming that temperature has minor effects on the interaction between DNA and nucleoprotein. The enhancement of ThT fluorescence in the presence of histones is also observed at pH = 7.2 (Figs. S4 and S6); however, the strength of the effect depends on buffer composition. In HEPES, the fluorescence growth is on the order of 20-fold, in close agreement with the data observed at native pH, while in TE buffer this increase is much more intense (40-fold). These findings highlight specific and non-specific interactions between buffer compounds and the species in solution, either biomolecules or the fluorescent dye. [39–41]Altogether, these observations indicate that, for the pHs investigated here, the overall behavior of histones and protamines regarding DNA condensation agrees with data obtained in ultrapure water where only DNA and nucleoproteins participate in the interplay. Therefore, the results above provide further evidence that, although histones and protamines exhibit physicochemical similarities such as high charge densities and large amounts of basic amino acids, they promote different supramolecular arrangements upon complexation with DNA.

3.3. Nano spectroscopy analyzes

Atomic force microscopy combined with infrared spectroscopy (AFM-IR) analyses were performed on DNA/nucleoprotein complexes to visualize the morphology of the aggregates and concomitantly obtain the vibrational signature of single nanoparticles. In Fig. 4, a topography image of DNA/protamine complexes indicates that the sample is populated by globular assemblies with heights mainly varying between 10 and 35 nm, and lateral dimensions reaching a few hundred nanometers in larger-sized particles. This result agrees with previous observations of Motta *et al.* in calf-thymus DNA/protamine complexes.[16] Most structures, however, have lateral sizes around ~50 nm, indicating that protamine forms very compact assemblies with DNA in agreement with its strong condensing capacity. Vibrational profiles collected from individual particles in the range 1550–1800 cm^{-1} bring information related to the amide band of proteins.[42] The infrared spectra shown in Fig. 4B are characterized by four vibrational bands located at 1634, 1652, 1668 and 1686 cm^{-1}. The most intense band, at 1652 cm^{-1}, could indicate either the presence of α-helix conformations or, more likely, disordered structures of protamine.[43] Another intense band appears at 1634 cm^{-1}, assigned to β-sheet

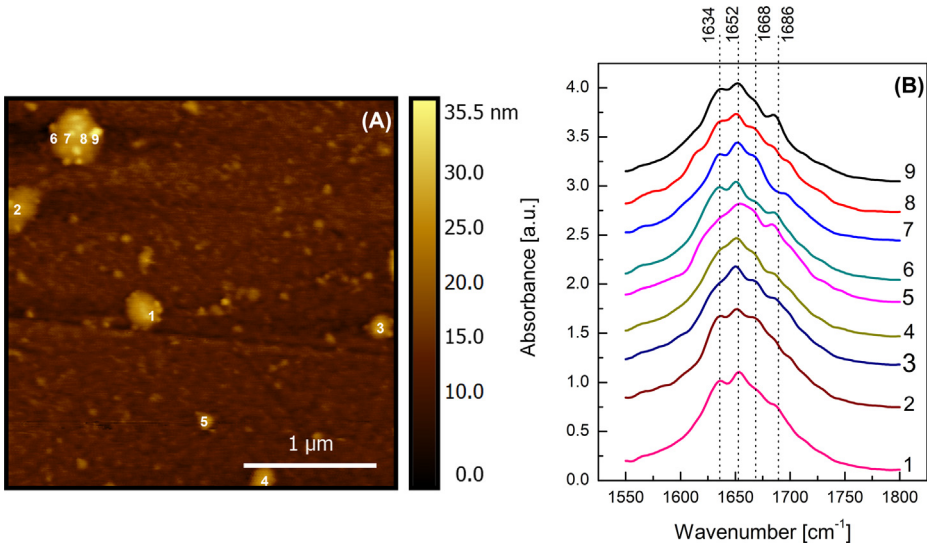

Fig. 4. AFM-IR data from DNA/protamine complexes. (A) Topography image showing highly compact globular condensates. (B) Infrared spectra from the areas indicated by corresponding numbers in (A). Spectra 1–5 were obtained from individual particles, and spectra 6–9 were collected from different regions of the largest globule.

conformations in the aggregates.[42,44] This band has already been reported in protamine-DNA complexes,[12] and the formation of these conformations is possibly favored by strong electrostatic interactions of protamine with DNA. Previous AFM-IR studies of our group conducted on polyelectrolyte systems formulated between DNA and cationic peptides also showed the presence of aggregates stabilized by β-sheet conformations.[25,27] One hypothesis for this recurrent feature is associated with the higher energetic stability of β-sheets compared to α-helices.[45] The other two bands have more complex assignments, however, vibrations at 1668 cm^{-1} are usually assigned to β-turns, while resonances at 1686 cm^{-1} can be assigned to anti-parallel β-sheets or, more commonly, to β-turns.[42] An interesting aspect to note in the spectra of Fig. 4B is that, although these four bands are observed at all selected points, it is possible to verify variations in relative intensity between the different peaks. This behavior suggests that the local composition of the nanoparticles contains different fractions of each conformation or that different protein/DNA ratios are found in distinct regions of the same nanoparticles.

In Fig. 5, it is shown AFM-IR data obtained from complexes prepared with histones. In contrast to protamine-based aggregates, the topographic image in 5A reveals structures primarily characterized by elongated fibers. The diameters of the larger fibers are around 250 nm, while several smaller structures are also observed with diameters around 150 nm. The heights vary from 30 to 60 nm and the lengths easily reach the micrometer scale. In addition to the fibrillar aggregates, some globules with sizes of a few tens of nanometers are also observed. The presence of fibrillar aggregates agrees with observations from fluorescence assays above, which revealed intercalation of ThT in ordered assemblies. In this case, the conformation into elongated assemblies could keep the inter base environment accessible to dye intercalation in DNA/histones complexes. In contrast, condensation into highly packed globules, observed in complexed with protamines, would hinder access of ThT to the structure of DNA strands.

The infrared spectra of the histone/DNA complexes are shown in Fig. 5B. Different bands across the amide I region are observed with the predominance of an intense peak at ~1650 cm^{-1}, which is ascribed to disordered conformations.[42,44] The spectra are also characterized by bands at ~1625 and 1684 cm^{-1}, related to the presence of β-sheets and β-turns, respectively. A faint band also appears around 1668 cm^{-1} in most spectra, indicative of turns. In addition, a peak around 1564 cm^{-1} is observed in the region of amide II. The unambiguous interpretation of this peak is controversial; however, it is associated with C=N vibrations, and some authors attribute it to β-turns.[46] As a whole, the infrared signature is similar to that observed in protamine complexes; however, in the case of protamines, the β-sheet content is higher. On the other hand, in the case of histones, we observed more significant variations between spectra extracted from different regions of the fiber. For example, the spectra corresponding to positions 4 to 8 in 5A, all obtained from the same fiber, show noticeable variations in relative intensities of peaks at 1645 cm^{-1} (disordered) and 1624 cm^{-1} (β-sheets), indicating that the fractions of these conformations may vary along the fiber.

3.4. Polarizing light microscopy (PLM)

DNA is a chiral molecule with a high degree of anisotropy and a persistence length on the order of 50 nm (or ~150 bp).[47] These chirality and anisotropy characteristics make DNA highly prone to form liquid-crystalline phases, especially at higher concentrations.[48] At concentrations typically found in chromosomes (i.e., 400–800 mg/ml),[49] DNA forms highly organized mesophases, with the appearance of cholesteric domains and hexagonal phases which have distinct optical responses under polarized light. We performed PLM assays on samples prepared in aqueous solutions using starting concentrations much lower than those observed in chromosomes. These samples were prepared from starting solutions in the range of a few mg/ml, at which the DNA appears isotropically distributed in solution, and no optical textures are identified under PLM. In Fig. 6, PLM images of condensates containing nucleoproteins show optically dense condensates with clear birefringent domains. The textures are characterized by oily streak patterns, alternating bright and dark regions, where local orientation determines the intensity of the light observed. By rotating the polarizer, it is also possible to observe a color response with respect to the orientation of the domains, where shades of blue appear in optically active regions indicating light retardation and highlighting the birefringent nature of these oriented domains. These textures are observed both in systems prepared with protamines and histones, and they are characteristic of liquid crystalline cholesteric or hexagonal phases.[50] In systems containing only DNA, cholesteric phases appear in concentration ranges

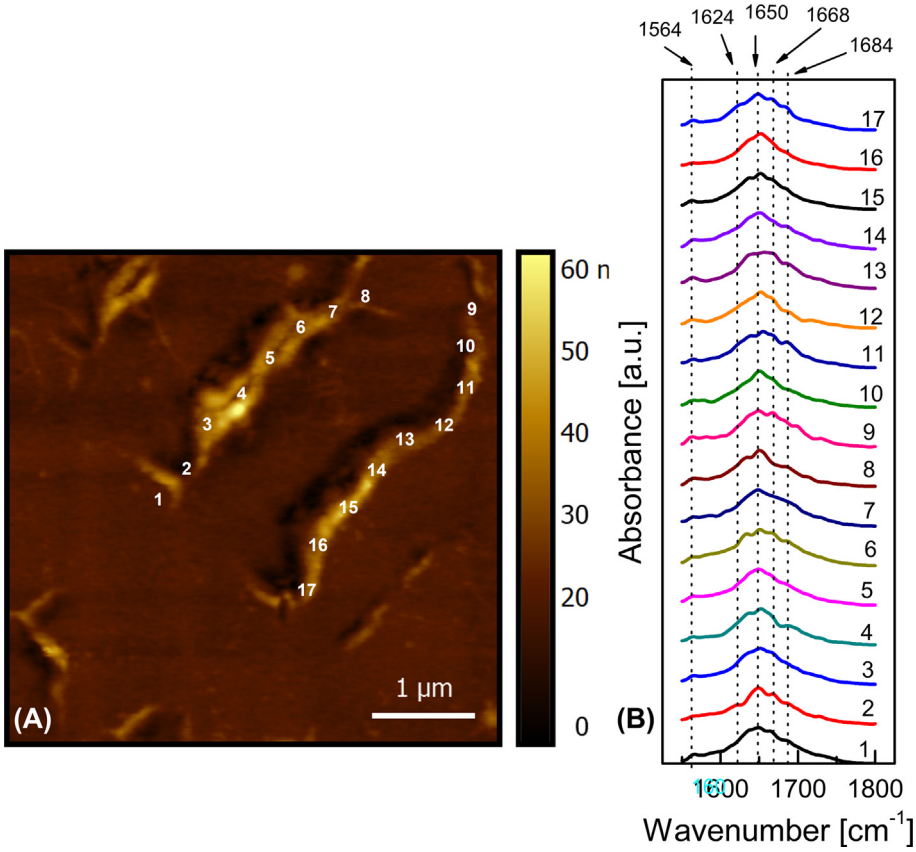

Fig. 5. AFM-IR data from DNA/histones complexes. (A) Topography image and (B) infrared spectra. Since the morphology of the complexes was characterized by elongated fibers, spectra were collected along the axis of the aggregates.

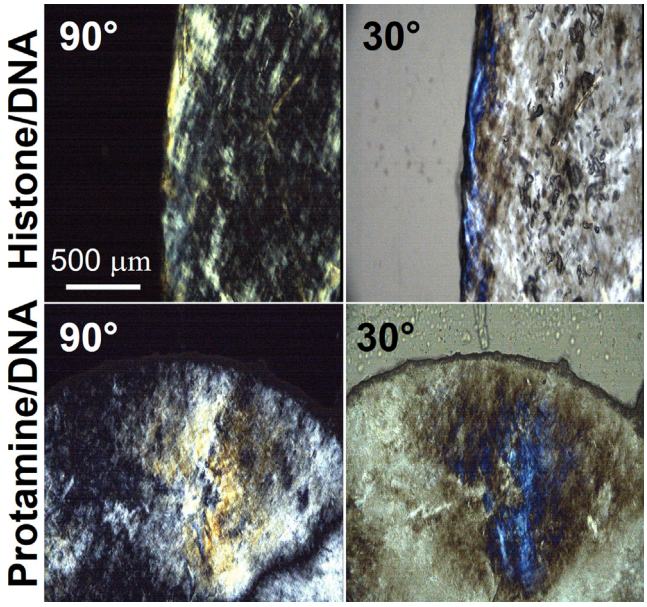

Fig. 6. Polarized light micrographs from condensates formed between DNA and histones (upper row), and protamines (bottom row). Oily streak textures appear due to oriented domains forming DNA mesophases. The angles shown in the figure indicate the rotation of the analyzer regarding the polarizer, and the presence of interference colors is a sign of retardation induced by the birefringent domains.

between ~160 and ~380 mg/ml and hexagonal phases are observed in the 380–670 mg/ml range.[50] Thus, our observations suggest that the condensates formed by nucleoproteins under the conditions employed here have compactness comparable to that observed in chromosomes.

3.5. Small-angle X-ray scattering

The inner structure of complexes formed between DNA and nucleoproteins was analyzed using SAXS. Under the experimental configuration used here, the structural information was obtained in the size range between ~1 and ~50 nm, thus within the nanometer scale and related to the supramolecular structure of the complexes. SAXS data from DNA/nucleoprotein condensates are shown in Fig. 7A and 7B. A key observation from these data is the appearance of new levels of organization in samples containing complexes compared to those containing only DNA or nucleoproteins (Fig. 7C-E). Indeed, the low-*q* range in DNA/nucleoprotein samples is featured by a linear decay that reveals a scaling law behavior typical of fractal aggregates.[29,51] At the higher angle region (i.e., $q > \sim 1\ nm^{-1}$), the profiles are characterized by Bragg peaks, indicating the formation of locally ordered domains upon complexation. The slope of the low-q region carries information on the fractal dimension of the scattering aggregates,[31] and the peak positions and widths bring information about the separation between correlated inhomogeneities within the complexes. Interestingly, remarkable differences are observed between condensates prepared with protamines or histones. Complexes prepared with protamines exhibit only one sharp peak at $q = 2.43\ nm^{-1}$, whereas complexes based on histones show a diffuse band at $q \sim 1.1\ nm^{-1}$ and a second peak at $q = 1.76\ nm^{-1}$. These features indicate that the nanoscale structure of complexes is strongly dependent on the type of nucleoprotein used in the preparation. To extract quantitative structural parameters, we have used the

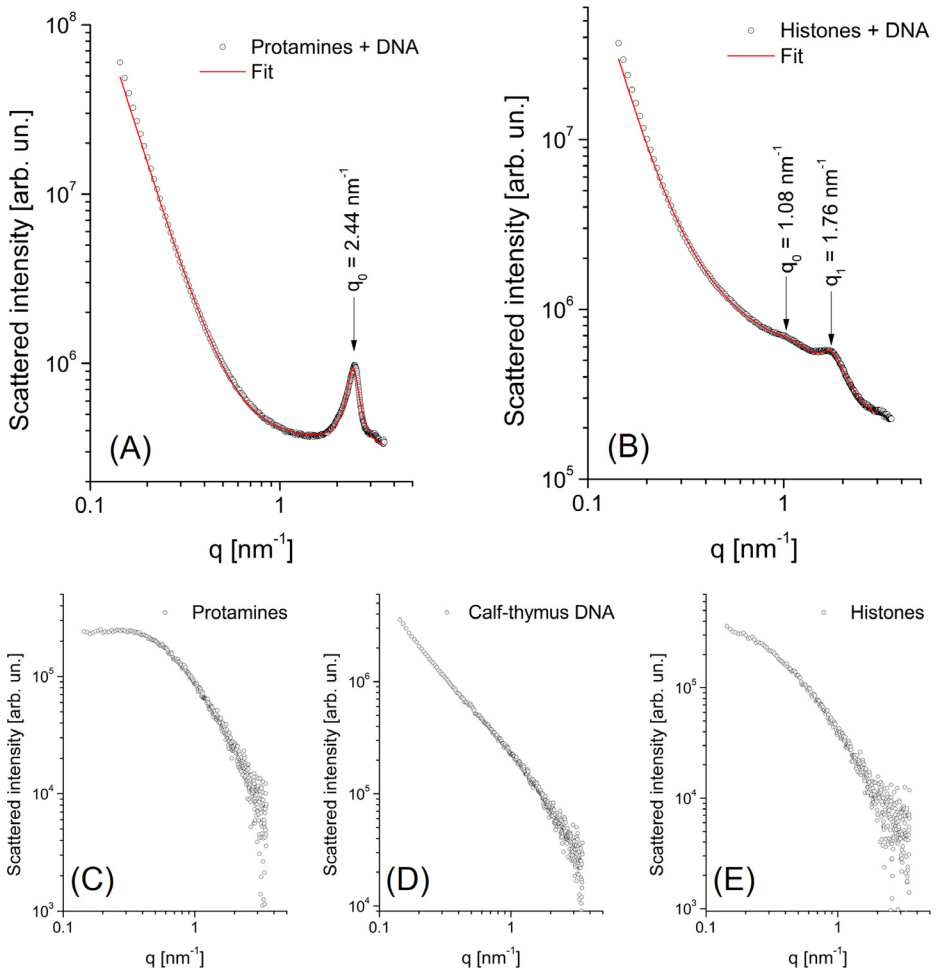

Fig. 7. SAXS data from samples prepared with (A) DNA/protamine condensates and (B) DNA/histone condensates. Red lines are model fits according to Eq. (2). In the bottom row, scattering data are from 1 mg/ml solutions prepared with (C) protamines, (D) DNA and (E) histones.

functional expression shown in Eq. (2) to fit the experimental data. From the results shown in Table 1, we observe that the low-angle region of DNA/protamine complexes is characterized by an exponent $\alpha = 3.6$, indicative of surface fractals (Fig. 7A).[27,31] The fractal dimension of these complexes could be straightforwardly determined through Eq. (4), leading to $D_s = 2.4$, which is associated with rough interfaces in DNA/protamine aggregates. The exponent β, related to the intermediate region roughly corresponding to lengths 5–10 nm, has values close to zero suggesting the presence of globular domains in the local structure of the aggregates. The interference peak at $q_0 = 2.43$ nm^{-1} corresponds to repeat distances of $d = 2\pi/q_0 = 2.6$ nm, very close to the diameter of hydrated DNA strands.[48] Therefore, we ascribe this result to the side-by-side organization of DNA duplexes within highly compacted domains. This configuration is consistent with AFM data, which revealed very compacted globules formed by DNA/protamine complexes. Furthermore, the fit indicates correlation lengths $\xi_0 = 5.2$ nm, i.e., two repeat distances on average. Although this SAXS information does not allow unambiguous determination of the three-dimensional organization within these aggregates, the separation $d = 2.6$ nm is compatible with distances between DNA chains in liquid crystalline phases, namely cholesteric and hexagonal phases.[2,52] Therefore, together with the texture information in polarized light microscopy, our data suggest that protamines promote the ordering of DNA chains into cholesteric symmetry arrangements.

Fig. 7B shows SAXS data from complexes formulated with histones. Curve data fitting with Eq. (2) revealed that the low-q region is featured by a decay exponent $\alpha = 4$, characteristic of sharp interfaces ($D_s = 2$). Furthermore, in the intermediate region, the decay exponent is $\beta = 0.88$, suggesting that in this case the scattering domains at length scales 5–10 nm have elongated geometries, in close agreement with AFM images which indicated the presence of elongated assemblies in DNA/histone complexes. The data are also characterized by a very diffuse peak centered at $q_0 = 1.08$ nm^{-1} followed by a more pronounced interference at $q_1 = 1.76$ nm^{-1}, respectively corresponding to 5.8 nm and 3.6 nm separations. These findings indicate that repeat distances in DNA/

Table 1
SAXS fitting parameters obtained from SAXS data.

Sample	α	D_s	β	q_0 [nm^{-1}]	ξ_0 [nm]	q_1 [nm^{-1}]	ξ_1[nm]	d [nm]
DNA/Protamine	3.6	2.4	0.08	2.43	5.2	***	***	2.58
DNA/Histone	4.0	2.1	0.88	1.08	3.4	1.76	1.1	3.59

histone condensates are larger than in protamine-based complexes, suggesting a lower level of compaction in the structure. Indeed, the correlation lengths associated with these peaks are found at ξ_0 = 3.4 nm and ξ_1 = 1.1 nm, lower than ξ values found in DNA/protamine assemblies, and coherent with a high degree of looseness in histone-based complexes.

4. Conclusions:

We presented a comprehensive study of DNA condensation mediated by histones and protamines, and found out that the mode of interaction and the supramolecular arrangement of the resulting complexes strongly depend on the kind of nucleoprotein used for condensation. The combination of AFM with infrared nano spectroscopy provided vibrational data from individual nanoparticles, revealing that β-sheet conformations predominantly stabilize the condensates. The presence of β-sheets is particularly remarkable in DNA/protamine complexes, whereas histone condensates have significant fractions of disordered domains with β-sheet fractions varying along fibrillar assemblies formed by these complexes. The increase of ThT emission yield in histone-based condensates indicates that these assemblies form ordered structures that preserve access of the dye to the inter base environment. In contrast, this effect is not observed in DNA/protamine complexes, consistent with highly packed structures where DNA folding hinders dye intercalation. These findings agree with the nanoscale morphology of the aggregates, which revealed the presence of elongated fibers in DNA-histone assemblies and globular structures in DNA-protamine complexes. SAXS data indicated the formation of correlated domains with DNA strands placed side-by-side in DNA/protamine assemblies and less correlated structures with larger inter-strand spacing in DNA/histone complexes. These findings also suggest a relevant role of the basic amino acids in the composition of protamines and histones. Indeed, protamines have arginine-enriched domains, with these residues composing nearly 67% of their sequence.[15] On the other hand, histones are much richer in lysines, and arginine residues correspond to only a tiny fraction of the amino acids in their composition. In this case, although the electrostatic attraction is a primary force driving complexation, the ability of arginine bidentate sidechains to establish multiple H-bonds should play a relevant role in reaching more packaged structures that hinder access to the inter base environment of DNA strands and lead to a diversity of secondary-structure conformations, including α-helices. The stronger condensing power of protamines is consistent with its biological function of compacting DNA into the nuclei of spermatic cells.[10] Also, tight packing is essential to preventing reactive oxidative species in sperm nuclei,[53,54] and hindrance of access to inter base microenvironment certainly contributes to avoiding DNA damage.

CRediT authorship contribution statement

Bruna B.S. Souza: Methodology, Investigation, Validation. **Thiago C. Lourenço:** Methodology, Validation, Investigation, Writing – review & editing. **Barbara B. Gerbelli:** Formal analysis, Investigation, Validation. **Pedro L. Oseliero Filho:** Formal analysis, Investigation, Validation. **Cristiano L.P. Oliveira:** Formal analysis, Investigation, Validation. **Antonio Miranda:** Conceptualization, Formal analysis, Writing – original draft. **Emerson R. da Silva:** Conceptualization, Formal analysis, Funding acquisition, Validation, Supervision, Writing – review & editing.

Data availability

Data will be made available on request.

Declaration of Competing Interest

The authors declare that they have no known competing financial interests or personal relationships that could have appeared to influence the work reported in this paper.

Acknowledgements

This work has received support from the Brazilian Research Council, CNPQ, through a fellowship to BBSS and a Universal grant to ERS (#409455/2018-0). ERS is a CNPQ productivity fellow (# 310916/2019-4). This study was financed in part by the Coordenação de Aperfeiçoamento de Pessoal de Nível Superior - Brasil (CAPES) - Finance Code 001, through a fellowship to TCL. The Sao Paulo Research Foundation (FAPESP) also supported this work through a Regular Grant to ERS (#2019/200907-7). P.L.O.F. acknowledges FAPESP (#2019/12301-1 and #2020/13204-7). B.B. G acknowledges FAPESP (#2018/05888-3 and #2020/02192-8). We are grateful to the National Nanotechnology Laboratory (LNNano) for awarding shifts for AFM measurements (#AFM-20220231), and Carlos Costa and Cleyton Biffe are kindly acknowledged for assistance during AFM data collection. Lucas Rodrigues de Mello (Biophysics, Unifesp) is kindly acknowledged for helping collecting data during AFM and SAXS assays. SAXS experiments were carried out on the SAXS-1 beamline of the Brazilian Synchrotron Light Laboratory (LNLS) under proposal #20190106, and we thank Florian Meneau for assistance.

Appendix A. Supplementary data

Supplementary data to this article can be found online at https://doi.org/10.1016/j.molliq.2022.120745.

References

[1] I.W. Hamley, V. Castelletto, Biological Soft Materials, Angew. Chem. Int. Ed. Engl. 46 (24) (2007) 4442–4455.
[2] A.C. Toma, M. de Frutos, F. Livolant, E. Raspaud, DNA Condensed by Protamine: A "Short" or "Long" Polycation Behavior, Biomacromolecules 10 (8) (2009) 2129–2134.
[3] D.J. Needleman, M.A. Ojeda-Lopez, U. Raviv, H.P. Miller, L. Wilson, C.R. Safinya, Higher-Order Assembly of Microtubules by Counterions: From Hexagonal Bundles to Living Necklaces, Proc. Natl. Acad. Sci. U. S. A. 101 (46) (2004) 16099–16103.
[4] J. DeRouchey, R.R. Netz, J.O. Radler, Structural Investigations of DNA-Polycation Complexes, Eur. Phys. J. E Soft Matter 16 (1) (2005) 17–28.
[5] L. van Dam, N. Korolev, L. Nordenskiold, Polyamine-Nucleic Acid Interactions and the Effects on Structure in Oriented DNA Fibers, Nucleic Acids Res. 30 (2) (2002) 419–428.
[6] C.L. Woodcock, R.P. Ghosh, Chromatin Higher-Order Structure and Dynamics, Cold Spring Harb, Perspect. Biol. 2 (5) (2010).
[7] J.A. Speir, J.E. Johnson, Nucleic Acid Packaging in Viruses, Curr. Opin. Struct. Biol. 22 (1) (2012) 65–71.
[8] T. Pfohl, Y. Li, J.H. Kim, Z. Wen, G.C. Wong, I. Koltover, M.W. Kim, C.R. Safinya, Biological Polyelectrolyte Complexes in Solution and Confined on Patterned Surfaces, Colloids Surf. a-Physicochem. Eng. Asp. 198 (2002) 613–623.
[9] X. Nie, Z. Zhang, C.H. Wang, Y.S. Fan, Q.Y. Meng, Y.Z. You, Interactions in DNA Condensation: An Important Factor for Improving the Efficacy of Gene Transfection, Bioconjug. Chem. 30 (2) (2019) 284–292.
[10] B. Alberts, Molecular Biology of the Cell, third ed., Garland Publishing, New York and London, 1994.
[11] Y. Liu, M. Guthold, M.J. Snyder, H. Lu, AFM of Self-Assembled Lambda DNA–Histone Networks, Colloids Surf. B Biointerfaces 134 (2015) 17–25.
[12] M.L.S. Mello, B.C. Vidal, Changes in the Infrared Microspectroscopic Characteristics of DNA Caused by Cationic Elements, Different Base Richness and Single-Stranded Form, PLoS One 7 (8) (2012) e43169.
[13] S. Gupta, N. Tiwari, M.A. Munde, A Comprehensive Biophysical Analysis of the Effect of DNA Binding Drugs on Protamine-Induced DNA Condensation, Sci. Rep. 9 (1) (2019) 5891.
[14] A. Boskovic, M.E. Torres-Padilla, How Mammals Pack Their Sperm: A Variant Matter, Genes Dev. 27 (15) (2013) 1635–1639.
[15] I. Maze, K.M. Noh, A.A. Soshnev, C.D. Allis, Every Amino Acid Matters: Essential Contributions of Histone Variants to Mammalian Development and Disease, Nat. Rev. Genet. 15 (4) (2014) 259–271.

[16] S. Motta, P. Brocca, E. Del Favero, V. Rondelli, L. Cantù, A. Amici, D. Pozzi, G. Caracciolo, Nanoscale Structure of Protamine/DNA Complexes for Gene Delivery, Appl. Phys. Lett. 102 (5) (2013) 53703.
[17] B.R. Madhanagopal, S. Zhang, E. Demirel, H. Wady, A.R. Chandrasekaran, D.N.A. Nanocarriers, Programmed to Deliver, Trends Biochem. Sci. 43 (12) (2018) 997–1013.
[18] M.K. Riley, W. Vermerris, Recent Advances in Nanomaterials for Gene Delivery — A Review, Nanomaterials 7 (5) (2017) 94.
[19] T. Nishinaka, A. Takano, Y. Doi, M. Hashimoto, A. Nakamura, Y. Matsushita, J. Kumaki, E. Yashima, Conductive Metal Nanowires Templated by the Nucleoprotein Filaments, Complex of DNA and RecA Protein, J. Am. Chem. Soc. 127 (22) (2005) 8120–8125.
[20] W.W. Wilfinger, K. Mackey, P. Chomczynski, Effect of PH and Ionic Strength on the Spectrophotometric Assessment of Nucleic Acid Purity, Biotechniques 22 (3) (1997) 474–481.
[21] N.C. Garbett, N.B. Hammond, D.E. Graves, Influence of the Amino Substituents in the Interaction of Ethidium Bromide with DNA, Biophys. J. 87 (6) (2004) 3974–3981.
[22] J.R. Casey, S. Grinstein, J. Orlowski, Sensors and Regulators of Intracellular PH, Nat. Rev. Mol. Cell Biol. 11 (1) (2010) 50–61.
[23] C.C. Decandio, E.R. Silva, I.W. Hamley, V. Castelletto, M.S. Liberato, V.X. Oliveira, C.L.P. Oliveira, W.A. Alves, Self-Assembly of a Designed Alternating Arginine/Phenylalanine Oligopeptide, Langmuir 31 (15) (2015) 4513–4523.
[24] E.R. Silva, E. Listik, S.W. Han, W.A. Alves, B.M. Soares, M. Reza, J. Ruokolainen, I. W. Hamley, Sequence Length Dependence in Arginine/Phenylalanine Oligopeptides: Implications for Self-Assembly and Cytotoxicity, Biophys. Chem. 233 (2018) 1–12.
[25] L.R. de Mello, L. Porosk, T.C. Lourenço, B.B.M. Garcia, C.A.R. Costa, S.W. Han, J.S. de Souza, Ü. Langel, E.R. da Silva, Amyloid-like Self-Assembly of a Hydrophobic Cell-Penetrating Peptide and Its Use as a Carrier for Nucleic Acids, ACS Appl. Bio Mater. 4 (8) (2021) 6404–6416.
[26] L.R. de Mello, I.W. Hamley, A. Miranda, W.A. Alves, E.R. Silva, β-Sheet Assembly in Amyloidogenic Glutamic Acid Nanostructures: Insights from X-Ray Scattering and Infrared Nanospectroscopy, J. Pept. Sci. 25 (6) (2019) e3170.
[27] L.R. de Mello, I.W. Hamley, V. Castelletto, B.B.M. Garcia, S.W. Han, C.L.P. de Oliveira, E.R. da Silva, Nanoscopic Structure of Complexes Formed between DNA and the Cell-Penetrating Peptide Penetratin, J. Phys. Chem. B 123 (42) (2019) 8861–8871.
[28] D. Necas, P. Klapetek, Gwyddion: An Open-Source Software for SPM Data Analysis, Cent. Eur. J. Phys. 10 (1) (2012) 181–188.
[29] J.S. Pedersen, Analysis of Small-Angle Scattering Data from Colloids and Polymer Solutions: Modeling and Least-Squares Fitting, Adv. Colloid Interface Sci. 70 (1997) 171–210.
[30] I. Bressler, J. Kohlbrecher, A.F. Thunemann, SASfit: A Tool for Small-Angle Scattering Data Analysis Using a Library of Analytical Expressions, J. Appl. Crystallogr. 48 (5) (2015) 1587–1598.
[31] B. Hammouda, Clustering in Polar Media, J. Chem. Phys. 133 (8) (2010) 84901.
[32] S. Kogikoski Jr., M.S. Liberato, I.M. Factori, E.R. da Silva, C.L.P. Oliveira, R.A. Ando, W.A. Alves, Polycaprolactone-Polyaniline Blend: Effects of the Addition of Cysteine on the Structural and Molecular Properties, J. Phys. Chem. C 121 (1) (2017) 863–877.
[33] R. Besselink, T.M. Stawski, A.E.S. van Driessche, L.G. Benning, Not Just Fractal Surfaces, but Surface Fractal Aggregates: Derivation of the Expression for the Structure Factor and Its Applications, J. Chem. Phys. 145 (21) (2016).
[34] P.O. Vardevanyan, A.P. Antonyan, M.A. Parsadanyan, H.G. Davtyan, A.T. Karapetyan, The Binding of Ethidium Bromide with DNA: Interaction with Single- and Double-Stranded Structures, Exp. Mol. Med. 35 (6) (2003) 527–533.
[35] S. Verma, V. Ravichandiran, N. Ranjan, Beyond Amyloid Proteins: Thioflavin T in Nucleic Acid Recognition, Biochimie 190 (2021) 111–123.
[36] P. Hanczyc, P. Rajchel-Mieldzioć, B. Feng, P. Fita, Identification of Thioflavin T Binding Modes to DNA: A Structure-Specific Molecular Probe for Lasing Applications, J. Phys. Chem. Lett. 12 (22) (2021) 5436–5442.
[37] A. Biancardi, T. Biver, A. Burgalassi, M. Mattonai, F. Secco, M. Venturini, Mechanistic Aspects of Thioflavin-T Self-Aggregation and DNA Binding: Evidence for Dimer Attack on DNA Grooves, PCCP 16 (37) (2014) 20061–20072.
[38] A. Biancardi, T. Biver, B. Mennucci, Fluorescent Dyes in the Context of DNA-Binding: The Case of Thioflavin T, Int. J. Quantum Chem. 117 (8) (2017) e25349.
[39] P. Pavani, K. Kumar, A. Rani, P. Venkatesu, M.J. Lee, The Influence of Sodium Phosphate Buffer on the Stability of Various Proteins: Insights into Protein-Buffer Interactions, J. Mol. Liq. 331 (2021).
[40] K. Roder, M. Schweizer, Running-Buffer Composition Influences DNA-Protein and Protein-Protein Complexes Detected by Electrophoretic Mobility-Shift Assay (EMSA), Biotechnol. Appl. Biochem. 33 (3) (2001) 209–214.
[41] A. Salis, L. Cappai, C. Carucci, D.F. Parsons, M. Monduzzi, Specific Buffer Effects on the Intermolecular Interactions among Protein Molecules at Physiological pH, J. Phys. Chem. Lett. 11 (16) (2020) 6805–6811.
[42] A. Barth, Infrared Spectroscopy of Proteins, Biochim. Biophys. Acta - Bioenerg. 1767 (9) (2007) 1073–1101.
[43] J.J. Pesek, F.R. Shabary, Investigation of Folding in Protamine by FTIR, Talanta 39 (10) (1992) 1215–1218.
[44] J. Kong, S. Yu, Fourier Transform Infrared Spectroscopic Analysis of Protein Secondary Structures, Acta Biochim. Biophys. Sin. (Shanghai) 39 (8) (2007) 549–559.
[45] A. Perczel, Z. Gáspári, I.G. Csizmadia, Structure and Stability of β-Pleated Sheets, J. Comput. Chem. 26 (11) (2005) 1155–1168.
[46] E. Goormaghtigh, J.M. Ruysschaert, V. Raussens, Evaluation of the Information Content in Infrared Spectra for Protein Secondary Structure Determination, Biophys. J . 90 (8) (2006) 2946–2957.
[47] W.M. Gelbart, R.F. Bruinsma, P.A. Pincus, V.A. Parsegian, DNA-Inspired Electrostatics, Phys. Today 53 (9) (2000) 38–44.
[48] I.W. Hamley, Liquid Crystal Phase Formation by Biopolymers, Soft Matter 6 (9) (2010) 1863–1871.
[49] J. Pelta Jr., D. Durand, J. Doucet, F. Livolant, DNA Mesophases Induced by Spermidine: Structural Properties and Biological Implications, Biophys. J . 71 (1) (1996) 48–63.
[50] A. Leforestier, F. Livolant, Supramolecular Ordering of DNA in the Cholesteric Liquid Crystalline Phase: An Ultrastructural Study, Biophys. J . 65 (1) (1993) 56–72.
[51] T. Zemb, P. Lindner, Neutrons, X-Rays and Light : Scattering Methods Applied to Soft Condensed Matter, first ed., Elsevier: Amsterdam, Boston, 2002.
[52] E. Raspaud, D. Durand, F. Livolant, Interhelical Spacing in Liquid Crystalline Spermine and Spermidine-DNA Precipitates, Biophys. J . 88 (1) (2005) 392–403.
[53] R.E. Braun, Packaging Paternal Chromosomes with Protamine, Nat. Genet. 28 (1) (2001) 10–12.
[54] J. DeRouchey, B. Hoover, D.C. Rau, A Comparison of DNA Compaction by Arginine and Lysine Peptides: A Physical Basis for Arginine Rich Protamines, Biochemistry 52 (17) (2013) 3000–3009.